Determining the seismic age of the young open cluster α Per

David Pamos Ortega[1], Antonio García Hernández[1], Juan Carlos Suárez[1], Javier Pascual Granado[2], Sebastià Barceló Forteza[1], José Ramón Rodón[2]
[1]*Departamento de Física Teórica y del Cosmos, Universidad de Granada, Campus de Fuentenueva s/n, 18071, Granada, Spain*
[2]*Instituto de Astrofísica de Andalucía (CSIC). Glorieta de la Astronomía s/n. 18008, Granada, Spain*

Accepted XXX. Received YYY; in original form ZZZ

ABSTRACT

The main objective of this work has been to develop a method to constrain the age of a young open cluster using seismic indices. This method consists of the following steps: 1) Extract the frequency content of a sample of stars in the field of an open cluster. 2) Search for possible regularities in the frequency spectra of δ Sct stars candidates, using different techniques, such as the Fourier transform, the autocorrelation diagram, the frequency difference histogram and the échelle diagram. 3) Build a grid of 1D rotating stars models using MESA for the evolution, and FILOU to calculate oscillating modes, to model those stars from which we have found a pattern of regularity in the frequency spectra. 4) Constrain the age of these stars using seismic indices: the low order large separation, the angular rotation frequency and the frequency of maximum amplitude. 5) Find possible common ages between these stars to determine the age of the cluster. For the analysis of the frequency content of pulsating stars, we have launched a new tool, MultiModes, accurate enough and more versatile, in terms of the control of the frequency analysis, than one of the most reliable and most used in the field, SigSpec. It has been tested with a sample of 32 stars in the field of the young open cluster Melotte 20, known as α Per, from which we have found 11 δ Sct stars, 9 of them never before labeled as such. We have obtained the low order large separation in four of them: TIC 410732825; TIC 354792288; TIC 285935852 and TIC 252829836. Two of these four stars, TIC 410732825 and TIC 285935852, show a splitting of frequencies in their frequency difference histogram, resulting in a possible angular rotation frequency of around 10 μHz. Considering that they are ZAMS stars, we have used the corresponding relation between the frequency of maximum amplitude and effective temperature to constrain, even more, the age of α Per between 103 and 131 Myr.

Key words: asteroseismology – delta Scuti stars

1 INTRODUCTION

Open clusters are laboratories of stellar and galactic astrophysics. Having at our disposal a group of tens of stars of similar chemistry and ages, within a narrow field of observation, allows us to better constrain models with which we can compare our observations. We can better characterize the stars in this way, determining their evolutionary stages and, by extension, the origin and evolution of the galaxy to which they belong.

There are many sources that can contribute to ambiguity determining the age of a cluster by isochrone fit on the HR diagram: uncertain distance modulus, cluster membership, binarity of individual stars, reddening and extinction, metallicity, different treatments of the physics of the models used to derive the theoretical isochrones, and the uncertainties from isochrone fit methods. Ambiguity is even greater in young clusters, with a sparse population of stars leaving the main sequence (turn off). On the HR diagram, it is the tip of the giants branch where a grouping of stars begin to burn the helium. They are used to date more evolved clusters.

Some types of classical pulsating stars, such as δ Sct stars, have a rich and varied frequency spectra. Space missions such as CoRoT (Baglin et al. 2006), Kepler (Koch et al. 2010) and TESS (Ricker et al. 2014) have lowered the detection threshold for their signals. Being grouped around the main sequence (MS), it is not easy to estimate the age with a small error by isochrone fit. In addition, it has been very difficult, until recently, to find regularities in the frequency spectra of these stars, as in the case of solar-type. There are studies showing that it is possible to find regularities in the frequency pattern of δ Sct stars, even out of the asymptotic regime (see for example, García Hernández et al. 2009; Paparó et al. 2016; Barceló Forteza et al. 2017; Bedding et al. 2020, and references therein). This is the named large separation, like for solar-type stars, but in the low order regime (from n=2 to n=8, Suárez et al. 2014). It is defined as the difference between modes of the same degree and consecutive orders:

$$\Delta\nu_{\rm low} = \nu_{\rm n,l} - \nu_{\rm n,l\text{-}1} \quad (1)$$

We used here the subscript *low* to differentiate it from that of the asymptotic regime. However, as in that case, this $\Delta\nu_{\rm low}$ is also related to the mean density of the star (Suárez et al. 2014; García Hernández et al. 2015, 2017).

Other seismic indices are the angular rotation and the frequency of maximum amplitude, directly related to the effective temperature (Barceló Forteza et al. 2018, 2020; Bowman & Kurtz 2018; Hasanzadeh et al. 2021) (BF2018, BF2020, BK2018 and H2021 from now on).

We study the possibility of constraining the age of a young cluster like Melotte 20 (also known as α Per), using such seismic indices. The

structure of the work is as follows: in section 2 we introduce the well studied open cluster α Per, to refer estimated ages in the literature. In section 3 we present the sample of stars with which we have done this research. In section 4 we introduce the code MultiModes, a new tool for the analysis of pulsating stars. In order to show its reliability, we have compared it to one of the most reliable and most used in the field, SigSpec (Reegen 2007). We explain the details of the code in this section, and also the comparative results obtained between them, using synthetic and real light curves, in terms of accuracy and computing time. In this section we also present the list of δ Sct stars candidates identified in our sample with the frequency analysis. In section 5 we show how, in four of them, it has been possible to measure the low order large separation. The angular rotation and the frequency of maximum amplitude of two of these stars have been measured. In section 6 we explain the details of the grid of pulsation models calculated with MESA (Paxton 2019) and FILOU (Suárez & Goupil 2008), in order to constrain the models that better fit to the seismic observations. In section 7 we compare the age found in our constrained models with other results obtained in other references, through isochrone fit. And so, we discuss the possibilities of this method to date young open clusters. Finally, in section 8, the main conclusions are exposed.

2 α *Per*

α Per is a young open cluster, located in the constellation of Perseus, at a distance of 174.89 ± 0.16 pc, obtained from Gaia DR2 parallaxes (Gaia Collaboration et al. 2018). Lodieu et al. (2019) have identified a total of 517 astrometric member candidates in the tidal radius of α Per, using a kinematic method combined with the statistical treatment of parallaxes and proper motions. The cluster members have solar metallicity (Netopil & Paunzen 2013), and it has an estimated extinction along the line of sight of around $A_V = 0.3$ (Prosser 1992).

It is supposed that because it is a nearby cluster, parameters are well determined. Cluster membership, determined from proper motions and parallaxes of the brighter stars, is better constrained than in distant clusters. In most nearby clusters, reddening is small, and overall metallicity is well known because they don't depart very much from the solar values. But there are really a lot of considerations that must be taken into account to calculate the luminosity and the effective temperature of an inhomogeneous sample of stars, in different evolutionary stages, in order to obtain accurate physical parameters. For example, the type of photometry to use, reddening, bolometric corrections and the correct modulus distance.

Recent age estimates by isochrone fit range from 20 to 90 Myr. Makarov (2006) estimates the age in around 52 Myr, fitting isochrone in the diagram M_V vs. (B-V), with Z = 0.02, E(B-V) = 0.055 and overshooting computed from the models by Pietrinferni et al. (2004). It is chosen the isochrone that best fit the most brighter star of the cluster, α Perseus. According to Silaj & Landstreet (2014), the age of α Per is $60 \pm 7 Myr$, determined with isochrones of Girardi et al. (2000), with Z = 0.02. They used an HR diagram considering that the uncertainties are less ambiguous than using a colour-magnitude diagram. Isochrones are most constrained around the one that passes throw the brightest main sequence star, ψ Per (HD 22192), which lies close to the turn off age main sequence (TAMS). In both works, the estimated age of the cluster is reliant on the parameters of a single star, with a difference of around 8 Myr in their results.

Lodieu et al. assumes an age of 90 Myr to compile the census of stars that are members of the cluster, noticeably older than Makarov and Silaj & Landstreet, because it is the most common age in the literature.

3 OUR SAMPLE

Firstly, we have done a cross match between VizieR Online Data Catalogue Gaia DR1 open cluster members (Gaia Collaboration et al. 2017) and TESS Input Catalogue (TIC) (Stassun et al. 2019), searching possible targets belonging to the same open cluster, from which we could obtain light curves from TESS mission. We have found a list of 112 stars in the field of α Per, with measured values for parallax, mean G magnitude, E(B-V) reddening, the bolometric corrections estimated by Andrae et al. (2018), and effective temperature. They all appear in the census prepared by Lodieu et al., obtained from Gaia Collaboration et al. (2018). We have estimated the G magnitude with equation:

$$M_G = G - 5logr + 5 - A_G \tag{2}$$

Distance r is taken as the inverse of the Gaia parallax. Extinction A_G is calculated from reddening values as in Stassun et al.:

$$A_G = 2.72E(B-V) \tag{3}$$

The G magnitude is converted to luminosity using the bolometric correction $BC(T_{eff})$ with the equation:

$$-2.5logL = M_G + BC_G(T_{eff}) - M_{bol\odot} \tag{4}$$

In Figure 1 we have plot an HR diagram with our sample. We have also included MIST[1] isochrones (Dotter 2016; Choi et al. 2016; Paxton et al. 2011, 2013, 2015), with solar metallicity, of different ages and rotational velocities. They all have been computed from the PMS phase to the end of hydrogen burning. In rotating models, solid-body rotation with $\Omega/\Omega_{crit} = 0.4$ is initialized at zero age mean sequence (ZAMS). Between using non rotating and rotating models, the evolutionary stage of a star is different with the same age. Rotation makes the star hotter or cooler depending on the efficiency of rotational mixing in the envelope. If rotational mixing introduces a sufficient amount of helium into the envelope, increasing the mean molecular weight, the star becomes more compact and hotter. On the contrary, if rotational mixing is not efficient, the centrifugal effect dominates, making the star cooler and more extended. The ages of the isochrones are taken to represent the values obtained by Makarov (2006), Silaj & Landstreet (2014) and Lodieu et al. (2019). We can see that all the calculated isochrones between 20 and 200 Mrs are quite overlapping in the MS zone. We also have located the position of ψ Per on the HR diagram, to find that it fits an isochrone of 200 Myr, quite far from the age estimated by Silaj & Landstreet. As for the star α Persei, used by Makarov, we have used the Hipparcos re-reduction parallax, and the mean reddening of the entire sample, since there is no Gaia parallax nor TIC reddening for this star. It is located quite far from the isochrones drawn on our diagram. Although the models appear to be correct because many of the stars in the sample are very grouped around the set of isochrones, we think that some of the measured parameters of α Per may be incorrect. This is another reason to think that seismic indices may be more reliable constraining the age of the cluster, taking into account the large number of considerations on which a good isochrone fit depends on.

We have analyzed a group of 32 stars using data from sector 18 of the TESS mission, with approximately 14700 points, a Rayleigh

[1] MESA Isochrones & Stellar Tracks

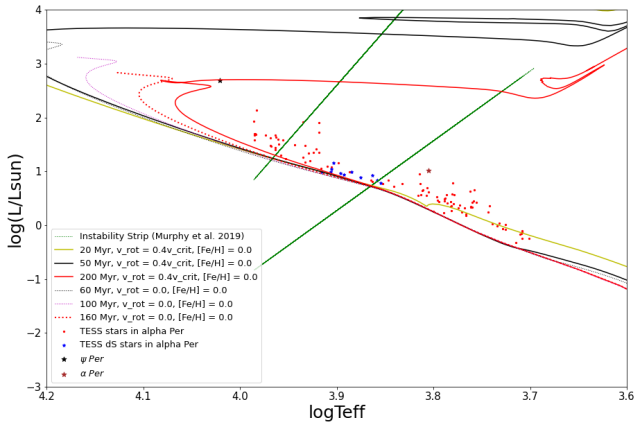

Figure 1. HR for the sample of 112 stars from the field of α Per, taken from TESS Input Catalogue. Isochrones between 20 and 200 Myr with solar metallicity are taken from MIST. (MESA Isochrones & Stellar Tracks). The borders of instability strip are also drawn, calculated according to Murphy et al. (2019). The position of ψ Per and α Perseus are also indicated, two of the most luminous stars in the cluster

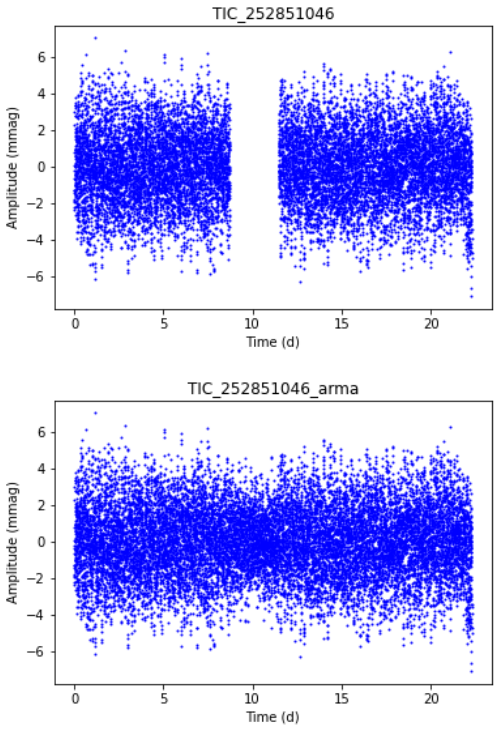

Figure 2. Top: Light curve for TIC 252851046. Bottom: Interpolated light curve for TIC 25851046 with MIARMA algorithm

resolution of approximately 0.045 d^{-1} an a cadence of two minutes. We have used the Pre-Search Data Conditioned (PDC) light curves, corrected for instrumental effects, that are publicly available through the MAST[2]. These light curves have a gap of about 6.2 hours duration, between TJD 1791.1115 and TJD 1791.3699, caused by the satellite downlink, when the spacecraft passed through the shadow of the Earth at start of orbit 43 (Figure 2). Pascual-Granado et al. (2015) showed that the analysis of light curves with gaps can produce an undesirable amount of spurious peaks. Thus, we decided to interpolate our data using the MIARMA code, which use autoregressive and moving average models. This method is aimed to preserve the original frequency content of the light curve, making the frequency extraction more reliable than leaving the gaps or using other gap-filling methods.

4 FREQUENCY ANALYSIS

4.1 MultiModes: a new tool for analysis of pulsating stars

Many of the light curves provided by space missions are uniformly sampled, but show some gaps, due to lack of observations, instrumental issues or enviromental effects. The Lomb Scargle Periodogram (from now on LS) is very powerful for analyzing non-uniformly sampled time series of data (Scargle 1982). It can be useful when the time series are uniformly sampled too, because the LS is reduced to the classical periodogram in this case. The algorithm calculate, at each frequency of interest, a time phase shift, and which in turn is used to evaluate the power spectra at that frequency. This time phase shift makes the LS to be independent of shifting all the points by any constant. In this way, the calculation of the LS is equivalent to performing a least squares fit of data to a sinusoidal function for each evaluated frequency. So there is a deep connection between the Fourier Transform and least squares analysis in the LS.

LS can be very slow in terms of computing speed, because it requires a number of calculations on the order of N^2, with N being the number of points in the sample. For this reason, it is implemented the Fast Lomb Scargle Evaluation (Press & Rybicki 1989), based on the extirpolation of data from an unevenly sample. The extirpolation consists of substituting the values of the series for others constructed by means of an evenly sampled mesh, so that the trigonometric sums that require the calculation of the periodogram approximate those of the original values. On this basis, the order of the calculations for the evaluation of the periodogram is reduced to NlogN.

The width of a peak does not depend on the number of sampled points or the signal to noise ratio (S/N), it only depends on Rayleigh resolution, which is inversely proportional to the total sample size (VanderPlas 2018). Two peaks within the Rayleigh resolution, in theory, could not be perfectly resolved by the periodogram. However, the stochastic nature of the series can cause numerous spurious frequencies to emerge, many of them of low amplitude but above the mean noise level. As detailed in the study by Balona (2014), the problem of using the pre-whitening technique lies in the large number of artificial frequencies that are generated with a high S/N. When, at each step, a signal very similar to the one to be extracted is added to the analyzed light curve, if not fit with enough accuracy, can generate an interference pattern around the added frequency.

These spurious frequencies can be avoided, to a great extent, by making a simultaneous fit to all the extracted frequencies, through non-linear optimization. By least squares fit to a multisine function, using as parameters the frequencies, amplitudes and phases of each of the peaks to be extracted.

The well-known SigSpec algorithm of Reegen (2007) (SS from now on) uses pre-whitening to extract all those frequencies that are above a certain criterion of significance, defined from the False Alarm Probability (FAP). Being a code widely used in asteroseismology, it is not currently an updated open source, easily accessible.

[2] Mikulski Archive for Space Telescopes

MultiModes (MM from now on) is a python routine developed to extract the most significant peaks of a sample of classical pulsating stars. It is available in public github repository[3] and it is customizable. This routine has been designed using the astropy packages [4] to calculate the periodograms and the lmfit packages [5] for the non-linear optimization of the extracted signals.

As show Figure 3, it takes as input a directory with corrected light curves, taken, for example, from the MAST archive, and the initial parameters written in a text file. Among these parameters are the maximum frequency of the studied domain (100 d^{-1} in δ Sct stars stars), the number of simultaneous peaks subtracted from the original light curve after the fit, or the stop criterion. With every light curve, the code calculates the frequency spectra, or periodogram, with the Fast Lomb Scargle algorithm. It extracts the highest amplitude peak and evaluates if it is real signal or due to noise, either by the FAP or by the S/N criterion, it is a decision of the user at the time of choosing the initial parameters. In this work we have chosen to use as stop criterion that S/N is greater than 4, following Breger et al. (1993), with which the results are much more similar to those of SS in terms of the number of extracted signals.

The algorithm fits frequency, amplitude and phase through non-linear optimization, using a multisine function. This function is redefined with the new calculated parameters. It does a simultaneous fit of a number of peaks (20 are usually enough).

Then they are subtracted from the original signal and goes back to the beginning of the loop with the residual, repeating the same process, until the stop criterion is reached. After that, the code can filter suspicious spurious frequencies, those of low amplitude above the Rayleigh resolution, and possible combinations of modes. The output, for every star, is a directory with the calculated periodograms, their corresponding residuals, and a text file with a list of the most significant detected modes, specifying the frequency, amplitude, phase, FAP or S/N ratio, and the corresponding minimum errors according to Montgomery & Odonoghue (1999).

4.2 Accuracy test with simulated spectra

To show the reliability of MM, we have tested with synthetic light curves. Following the work of Balona (2014), we have constructed these curves with 50, 100, 200 and 400 frequencies, with uniformly distributed values between 0 and 30 d^{-1}, amplitudes ranging between 0 and 10 mmag, exponentially distributed towards low values, phases uniformly distributed, and adding a Gaussian noise of about 0.5 mmag. Figure 4 show a comparative analysis of accuracy between MM and SS with the extracted peaks. The frequency deviation of MM is similar to that of SS in the curves with 50 and 100 frequencies, around 10^{-4} d^{-1}, when we used an unlimited number of components for the simultaneous fit of the simulated signal. With a higher number of frequencies, 200 and 400, SS is more accurate than MM by one order of magnitude, because MM used a limited number of components for the simultaneous fit, no more than 50. As the frequency density increases, the problem becomes more unstable as more and more spurious frequencies appear, with both MM and SS. Therefore, it makes sense to limit the number of components of the simultaneous fit of the light curve when frequency density is very high. In this sense, MM allows us to have greater control over the frequency analysis, by being able to limit the number of components for the fit, and work by packages, which we cannot do with SS.

[3] MultiModes
[4] The Astropy Project
[5] LMFIT

Table 1. Comparative analysis between SS and MM extracted peaks, using interpolated light curves with ARMA, for the 11 δ Sct stars sample from α Per. N_{SSar} and N_{MMar} are, respectively, the number of extracted frequencies by SigSpec and MultiModes. SSarMMar is the degree of coincidence between SigSpec and MultiModes

TIC	N_{SSar}	N_{MMar}	SSarMMar
104319359	249	238	97.9
116011834	233	222	97.7
252829836	82	76	97.4
252851046	213	222	93.7
285935852	45	40	97.5
347570557	189	188	94.7
354638295	97	89	98.9
354792288	55	47	100.0
401079326	39	35	100.0
410732825	69	55	100.0
428320122	71	64	100.0

4.3 Frequency content of the δ Scuti sample

From the sample of 32 analysed stars with MM, we have found that 11 of them are δ Sct stars stars, or hybrids, a type of pulsating stars with intermediate mass that show low order acoustic oscillations (p-modes) and also high order gravity modes (g-modes), more typical of γ Dor stars (Grigahcène et al. 2010; Uytterhoeven et al. 2011). Except TIC 252829836 and TIC 347570557, 9 stars in our sample had not been labeled as δ Sct stars before this work.

We have analysed the frequency content of these 11 stars using MM and SS, for greater reliability. When comparing the frequencies extracted by the two codes, we have considered that an MM frequency is equal to an SS frequency when both are closer than the Rayleigh resolution. We have established the degree or percentage of coincidence based on whether each frequency extracted by MM appears or not among those extracted by SS. As we can see in Table 1, the degree of coincidence between MM and SS in the values of the extracted frequencies, extracting the most significant frequencies, is above 90% in all the cases.

5 SEISMIC INDICES OF δ *Scuti* STARS

Among our sample of 11 δ Sct stars stars, in four of them, TIC 410732825, TIC 354792288, TIC 285935852 and TIC 252829836 (Figure 5), we have found a pattern that we identify as a low order large separation ($\Delta\nu_{low}$). We have followed the techniques de-

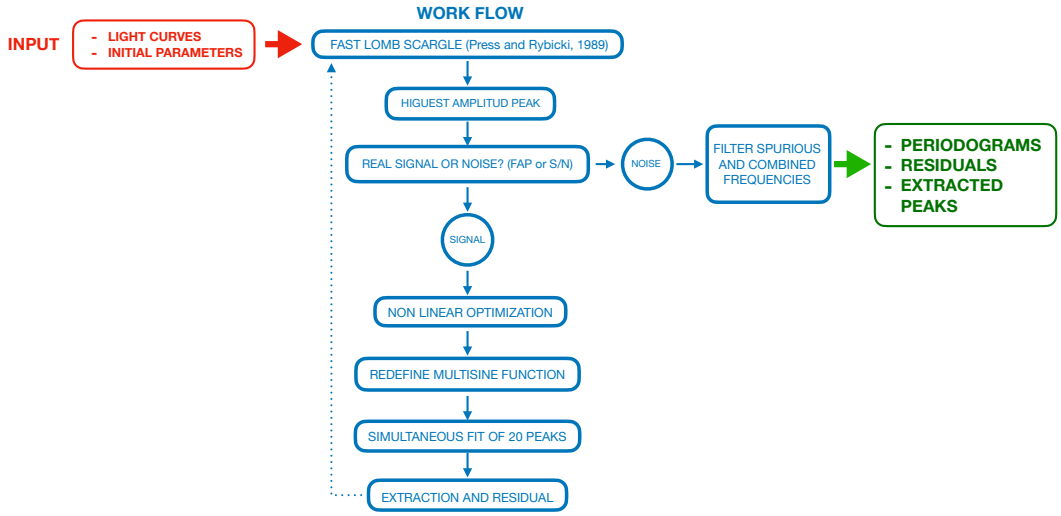

Figure 3. Workflow of the MultiModes algorithm

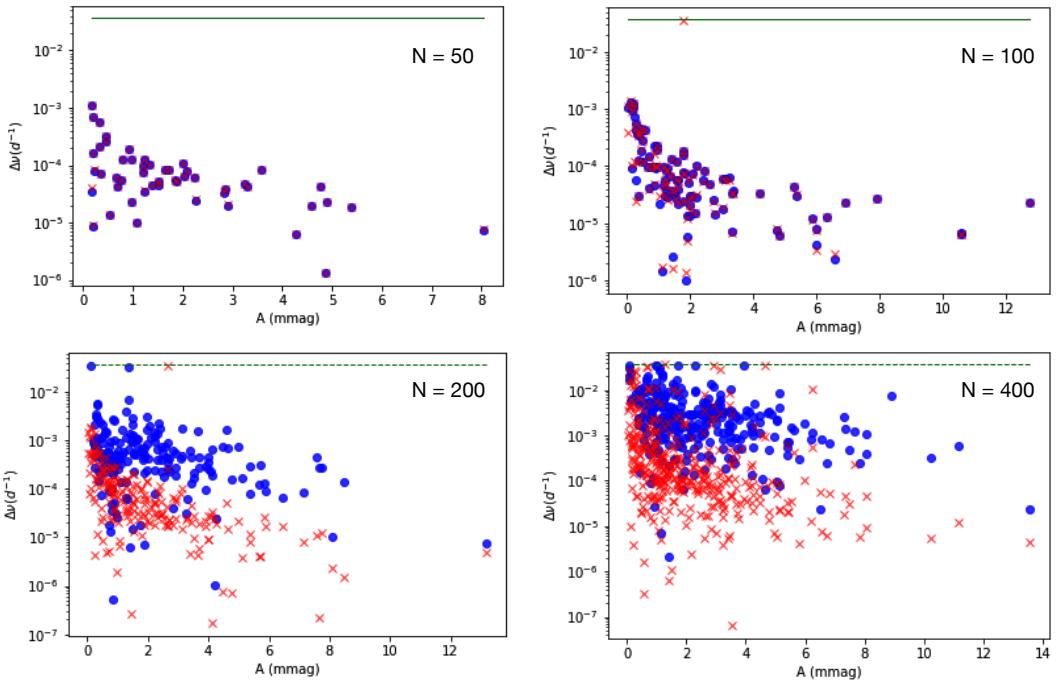

Figure 4. Comparative analysis of accuracy between MM and SS, using simulated light curves with different number of frequencies, 50 (upper left panel), 100 (upper right panel), 200 (bottom left panel) and 400 (bottom right panel). Each plot represents the frequency deviation of the extracted peaks with MM (blue filled circles) and SS (red crosses). The dotted green line is the level of the Rayleigh resolution

scribed in García Hernández et al. (2009) and Ramón-Ballesta et al. (2021).The autocorrelation function (AC), the Fourier transform (FT), the histogram of differences of frequencies (FDH), and the échelle diagram (ED) were applied to the 30 frequencies with highest amplitudes and above 5 d^{-1} to avoid g modes. These frequencies are selected by amplitude but are given equal amplitudes when computing the transformations.

Figure 6 show the case of TIC 354792288 (see the other three stars in Appendix A). The FT, AC and FDH show a peak around 42 μHz. It may be half the value of the low order large separation. AC and FDH also show a peak around 84 μHz. The ED shows the alignment of several frequencies when 84 μHz is chosen as the low order large separation.

We also searched for a pattern connected to the rotational splitting in the p mode regime. At first order in the perturbative theory, rotation splits the oscillation modes of the same order and the same degree, in the form:

$$\omega_{nlm} = \omega_{nl} + m\Omega \tag{5}$$

Being ω the angular frequency and Ω the angular rotation frequency.

This would allow to find a pattern corresponding to the rotation frequency in the periodogram, i.e., a regular structure related to Ω. However, this simple distribution of frequencies is only valid for slow rotators. Even at moderate rotations (around 50 km s^{-1}) the picture changes: rotational splitting is not symmetric anymore and ever the centroid can move (see for example, Suárez et al. 2006). These effects hamper the identification of a rotational splitting.

None the less, some theoretical works computing 2D non-pertubative models and rapid rotation combined the AC and the FT following García Hernández et al. (2009) to search for the patterns of the large frequency separation and the rotational splitting (Reese et al. 2017). They pointed out that the large separation or its half value appears usually clearer in the FT, whereas twice the rotational splitting can be found better in the AC. Additionally, others have found combinations between the large separation and the rotational splitting (Evano et al. 2019).

From the observational side, Paparó et al. (2016) searched for regularities in the frequency spectra of δ Sct stars stars observed by CoRoT using a visual inspection and by means of a semi-automatic algorithm that look for spacings between frequencies. They argued that some of these spacings might be not only the large separation but also the rotational splitting or a linear combination of both. The work of Barceló Forteza et al. (2017) uses AC, FDH and ED for finding rotational splittings with a sample of four δ Sct stars stars, with the idea of supporting the thesis that structural characteristics of the star, such as rotation, alter the power spectra, particularly in the flat plateau, where density of low amplitude frequencies increases with the rotation rate. Ramón-Ballesta et al. (2021) related regularities found in the frequency spectra of binary δ Sct stars to the rotational splitting. In their work, they used the FT, the AC and the FDH as in our research.

The FDH for two of our stars, TIC 410732825 (Figure 7) and TIC 285935852 (Figure A.2), show a splitting of frequencies, and both show a prominent peak in the histogram, that could be the angular rotation, of around 9-11 μHz. In the case of TIC 285935852, Figure 8 represents the periodogram with the most visible modes, between 40 and 60 μHz. It is shown the low order large separation, with a value of around $\Delta\nu_{\rm low} = 7d^{-1}$. Some rotational multiplets are also visible, which give the clue about the value of the rotation speed of the star, according to Equation 5, of around 0.9-1.0 d^{-1}, or equivalently, 9-11 μHz. The modes distribution is compared to a suitable model calculated with MESA-FILOU (see section 6. Some modes seem to follow the frequency distribution of the model. Others, related to rotation, don't do it. Even the centroids of the multiplets are displaced from the model. So we must be careful using non-rotating models, as it is done in the work of Murphy et al. (2021) (submitted), where they perform a mode identification with five δ Sct stars located in the Pleiades. Even for moderate rotating stars like TIC 285935852, it is found that there are important effects, not only in the simple modulation of the splitting, but there are also second order effects, which shift the centroid, breaking the symmetry on the modes with m different from zero. However, our models are reliable enough to believe the observed seismic indices and some oscillating modes.

Another seismic index is the frequency of maximum amplitude, related to the effective temperature of the star, as shown in the works of BF2018, BF2020, BK2018 and H2021. This relation is very dependent on the evolutionary stage of the star and dispersion can be very high in some cases. There are different ways of defining the frequency of maximum amplitude. Balona & Dziembowski 2011 defines it with the peak of maximum amplitude in the spectrum, $\nu_{\rm max,0}$. BF2018 do it through the amplitude weighted mean of all the most significant extracted peaks, $\nu_{\rm max,w}$, and H2021 through the maximum of the autocorrelation of the power spectra correlation, $\nu_{\rm max,2D}$. TIC 354792288 and TIC 285935852 show a set of very grouped frequencies between 40 and 60 μHz (Figure 10), that seems not to be mixed modes because they may be propagating near the surface of the star. With both stars, we use $\nu_{\rm max,0}$ from BF2018 and BK2018, $\nu_{\rm max,w}$ from BF2020, and $\nu_{\rm max,2D}$ from H2021, in order to determine the age of these stars. Table 2 shows the values of the seismic indices that will serve to constrain the models as much as possible to try to date these four stars, and therefore, the cluster.

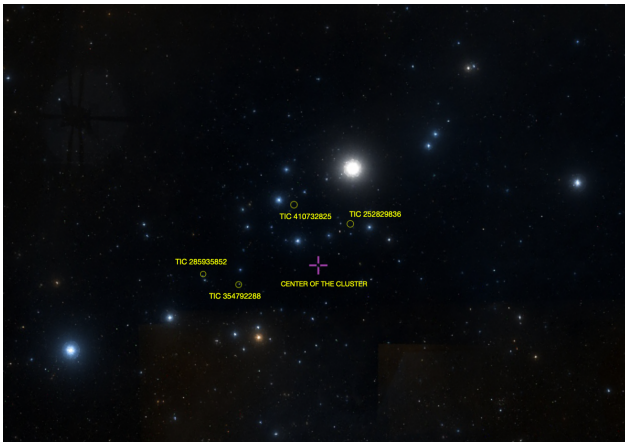

Figure 5. The four selected targets in the field of α Per from which we have obtained regularities in the frequency spectra

Table 2. Seismic indices of the selected targets from α Per to constrain the models, in order to determine its ages

TIC	$\Delta\nu_{\rm low}\,(d^{-1})$	$\omega_r\,(\mu Hz)$	$\nu_{\rm max,0}\,(\mu Hz)$	$\nu_{\rm max,w}\,(\mu Hz)$
410732825	63 ± 1	10 ± 1	-	-
354792288	83 ± 1	-	671 ± 1	623 ± 1
285935852	82 ± 1	10 ± 1	625 ± 1	579 ± 1
252829836	71 ± 1	-	-	-

6 THE GRID OF MODELS

For this purpose, we have built a grid of 1D stellar models using the code MESA (Paxton 2019), for the evolution, and FILOU (Suárez & Goupil 2008) for calculating the oscillating modes, because it takes into account the stellar distortion due to the centrifugal force in the oscillation frequency computation, and rotation up to second order in the perturbation approximation, including near-degeneracy effects. We have taken orders $2 \leq n \leq 8$ and degrees $0 \leq l \leq 2$, for calculating the low order large separation of the models.

About MESA models, we have built the grid using the parameters of Table 3, delimiting ages between 20 and 200 Myrs. According to $Z_{\rm base}$ values, we have selected the Type2 tables for opacities. For the mixing length parameter we have taken the default value, $\alpha = 2.0$. In relation to diffusion coefficient for mixing of material, $D\_mix = 1/30$ (Heger et al. 2000).

In total, 24965 models were calculated. We have constrained them

[3] Echelle 1.5.1

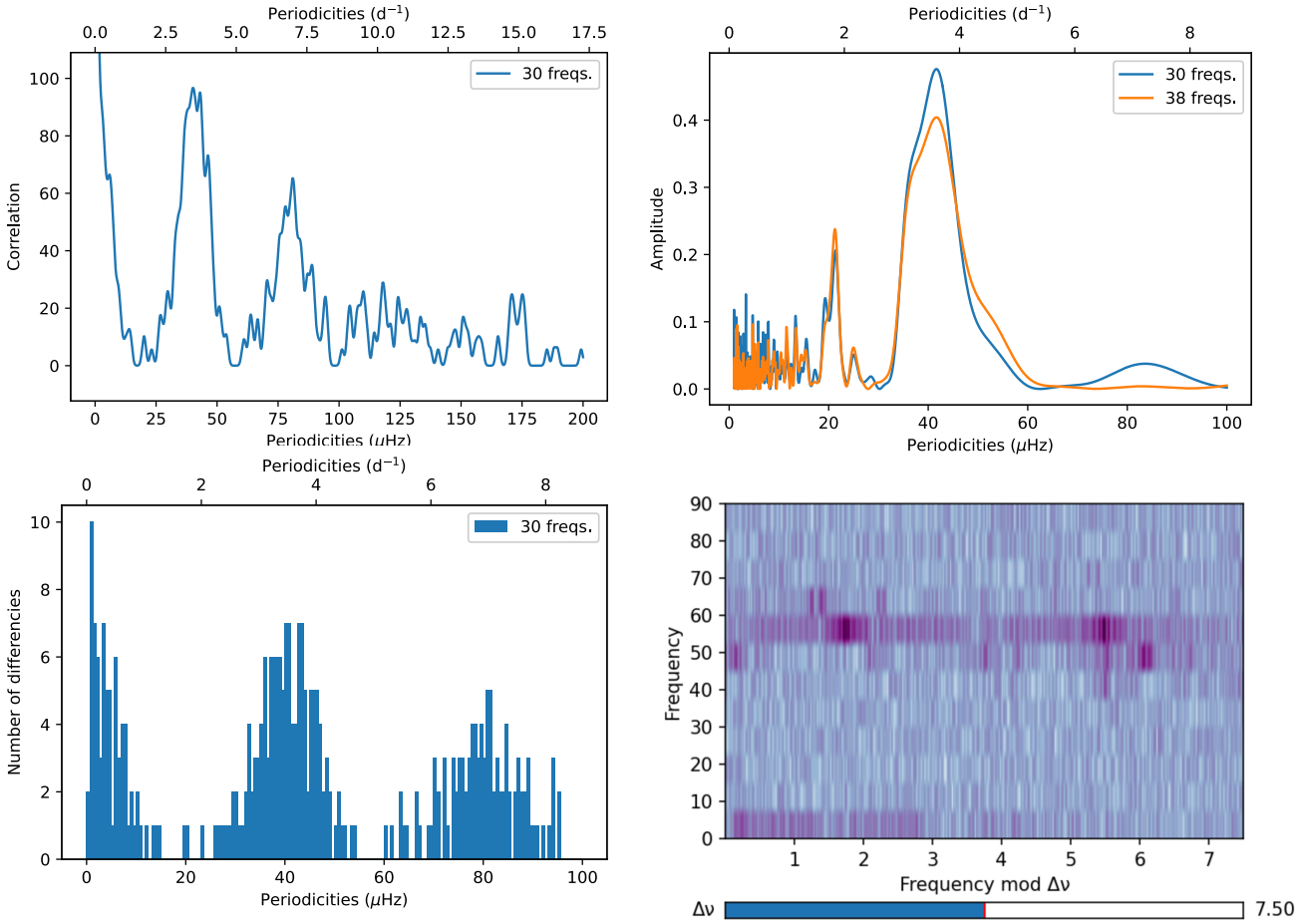

Figure 6. Measured regularities in the frequency spectra of TIC 354792288. The top left panel represents the autocorrelation diagram (AC) of periodicities calculated with the first 30 frequencies extracted by MM, showing peaks around 42 μHz and 84 μHz. Top right, the Fourier transform (FT) for the periodicities of those first 30 frequencies, showing a peak around 41 μHz. Bottom left, the frequency difference histogram (FDH) with the first 30 frequencies, showing peaks around 41 μHz and 82 μHz. Bottom right, the échelle diagram (ED) showing a very clear vertical ridge around 7.5 d^{-1}, equivalent to around 86 μHz. ED is done with Python package Echelle 1.5.1, developed by Hey & Ball 2020[3]

Table 3. Selected values for the parameters of the grid of models built with MESA

Parameter	Range	Step
Age	[20, 200] Myr	1 Myr
M ($M_\odot$)	[1.6, 2.6]	0.1 $M_\odot$
Z_0	[0.010, 0.020]	0.002
Ω/Ω_c	[0.10, 0.25]	0.05
α	2.0	Fixed

by the seismic indices as explained in above section (Table 2), assuming they are all members of the cluster, and solar metallicity.

7 SEISMIC DETERMINATION OF THE AGE OF α *Per*

Figure 10 shows the effective temperature vs age plots for all the calculated models, using the relationships between the maximum amplitude frequency and the effective temperature exposed in section 5, and without using any. The constrained models for TIC 410732825 are represented in green, for TIC 354792288 in blue, for TIC 285935852 in red and for TIC 252829836 in orange. If we do not use any kind of relationship between the maximum amplitude frequency and the effective temperature to constrain the ages of our four stars (top left panel), then the age of the cluster would be between 103 and 160 Myr. If we use the $\nu_{\rm max,w}$-$T_{\rm eff}$ relationship from BF2020 (middle right panel) or $\nu_{\rm max,2D}$-$T_{\rm eff}$ from H2021 (bottom left panel), then the constrained models for our four stars do not show common ages. However, in the case of BF2020, the possible ages for TIC 410732825 and TIC 354792288 are separated by a difference of just 2-3 million years, which is too narrow to rule out the possibility that they may overlap around a common age of about 100 Myr.

And finally, if we use the $\nu_{\rm max0}$-$T_{\rm eff}$ relationship from BF2018 (top right panel) and BK2018 (middle left panel), the result is that α Per could have an age between 103 and 131 Myr.

Table 4 shows the observed values of the main parameters of these four stars, and Table 5 the values corresponding to the constrained models. Regarding TIC 410732825, the models tell us that it has a larger radius and a lower density than the calculated from the observed parameters. The density obtained from the large separation using the García Hernández et al. (2017) relationship seems to corroborate this. The values of the projected rotation of Kounkel et al.

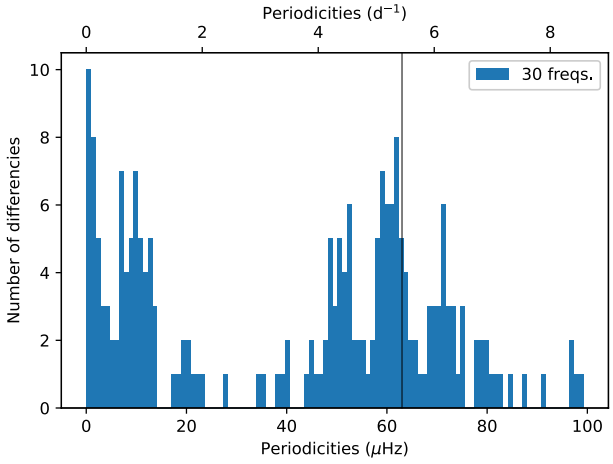

Figure 7. The FDH for TIC 410732825, showing a splitting of frequencies of the same order and degree and a possible angular rotation of around 9-11μHz. Black line indicates the measured value of the low order large separation, around 63 μHz

(2019) and the seismic rotation are very similar, so the star seems to be equator on. This would explain why the possible values of the observed luminosity are below those of the models. If the observed parameters for TIC 252829836 were correct, then the star would be hundreds of millions of years age, to be in agree with the measured large separation. Therefore, we discard this option to think that some parameters of this star may not be well determined.

Compared to these works, our four stars, that seem to be members of the cluster, according to Lodieu et al. (2019), and not seem to be binary systems, according to Kounkel et al. (2019), point to an older age for the cluster, at least 103 Myr. There are more sources of uncertainty using the isochrone fit method than the one we propose here based only on seismic indices, and with no need of doing frequency mode identification. The grid we have used can be extended to take into account the variability of parameters such as overshooting, the mixing length parameter or the diffusion of angular momentum, which have been taken with the values exposed in section 6.

In our study, only two stars really delimit the possible age ranges for the cluster, TIC 410732825 and TIC 354792288 (Figure 10). In the case of the low order large separation and the angular rotation frequency, they can be determined with great accuracy in favorable cases such as with these two stars. Adding the maximum amplitude frequency to relate it to the effective temperature can help to constrain the models, but the uncertainty is large. This relationship needs to be improved so that constrained models are as reliable as using only the low order large separation and rotation frequency. In any case, the estimated age for α Per must be considered with all caution, pending that even more detailed studies, which could include the asteroseismic values of a greater number of stars, may or may not confirm our result. We trust this is a promising method for dating young star clusters.

8 CONCLUSIONS

We have tested a method in order to determine the age of the young open cluster α Per. The technique is based on finding seismic indices, such as the low order large separation, the frequency of maximum amplitude and the rotation frequency in a sample of 11 δ Sct stars stars belonging to the field of the cluster. With them we have used the FT, the AC, the FDH and the ED. In four of them, TIC 410732825, TIC 354792288, TIC 285935852 and TIC 252829836 we have measured the low order regime large separation. With TIC 410732825 and TIC 285935852 we have found evidences of the angular rotation frequency. With the necessary caution, considering that they are ZAMS stars, we have used the relations between the frequency of maximum amplitude and the effective temperature (BF2018, BK2018, BF2020 and H2021), to try to constrain, even more, the age of α Per between 103 and 131 Myr.

For the frequency analysis, we have launched a new code written in python, MM (MultiModes), that show a good reliability after testing with synthetic light curves, and after being compared with one of the most reliable codes in the field, SS. Moreover, MM is more versatile in terms of frequency analysis control. It has allowed us to find nine new δ Sct stars stars from the original sample of 32 analysed stars.

In next works we hope to continue testing this technique with other similar clusters, to consolidate the use of seismic observables to try to date stars as accurately as possible.

ACKNOWLEDGEMENTS

This publication is part of the project "Contribution of the UGR to the PLATO2.0 space mission. Phases C / D-1", funded by MCNI/AEI/PID2019-107061GB-C64.

JPG acknowledges funding support from Spanish public funds for research from project PID2019-107061GB-C63 from the "Programas Estatales de Generación de Conocimiento y Fortalecimiento Científico y Tecnológico del Sistema de I+D+i y de I+D+i Orientada a los Retos de la Sociedad", as well as from the State Agency for Research of the Spanish MCIU through the “Center of Excellence Severo Ochoa” award to the Instituto de Astrofísica de Andalucía (SEV-2017-0709).

AGH acknowledges funding support from Spanish public funds for research under project PID2019-107061GB-C64 by the Spanish Ministry of Science and Education, and from ‘European Regional Development Fund/Junta de Andalucía-Consejería de Economía y Conocimiento’ under project E-FQM-041-UGR18 by Universidad de Granada.

This paper includes data collected with the TESS mission, obtained from the MAST data archive at the Space Telescope Science Institute (STScI). Funding for the TESS mission is provided by the NASA Explorer Program. STScI is operated by the Association of Universities for Research in Astronomy, Inc., under NASA contract NAS 5–26555.

DATA AVAILABILITY

Tables of the most significant peaks, corresponding to each of the 11 δ Scuti stars of our sample, extracted with MM, are available in VizieR DataBase. In them we can find the values of the frequencies, amplitudes, phases, corresponding errors and S/N of the extracted peaks.

REFERENCES

Andrae R., et al., 2018, A&A, 616, A8

Baglin A., Michel E., Auvergne M., COROT Team 2006, in Proceedings of SOHO 18/GONG 2006/HELAS I, Beyond the spherical Sun. p. 34

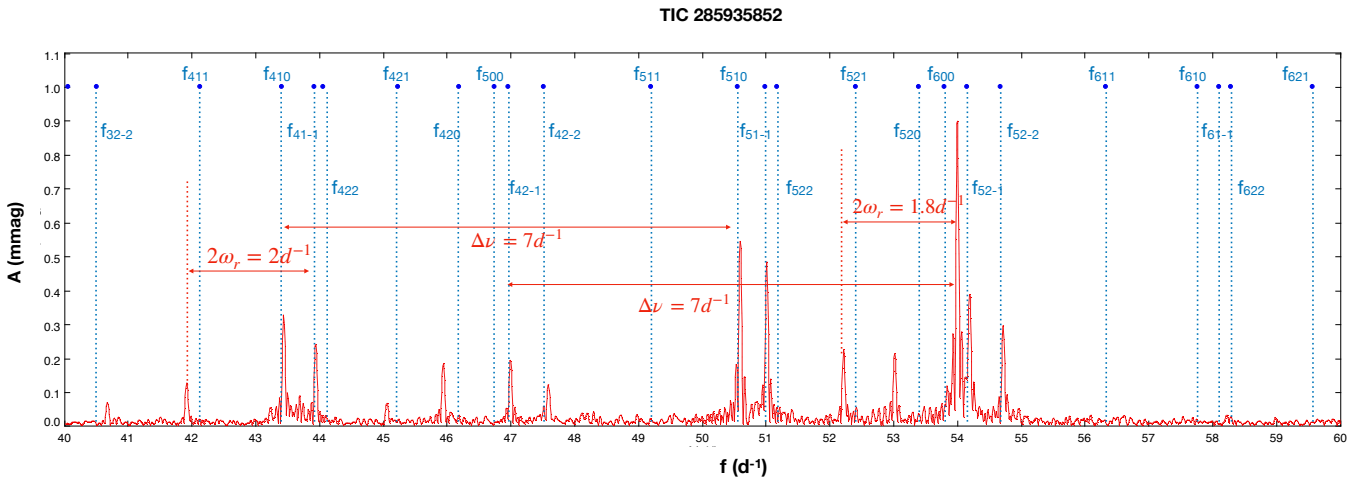

Figure 8. Periodogram of TIC 285935852, showing a measured low order large separation of around $\Delta\nu_{\rm low} = 7d^{-1}$, and a rotational splitting of around $\omega_r = 1.9d^{-1}$. The modes distribution is compared to a suitable model calculated with MESA-FILOU (see section 6. Some modes seem to follow the frequency distribution of the model. Others, related to rotation, where the frequency splitting is visible, no. Even the centroids are displaced from the model

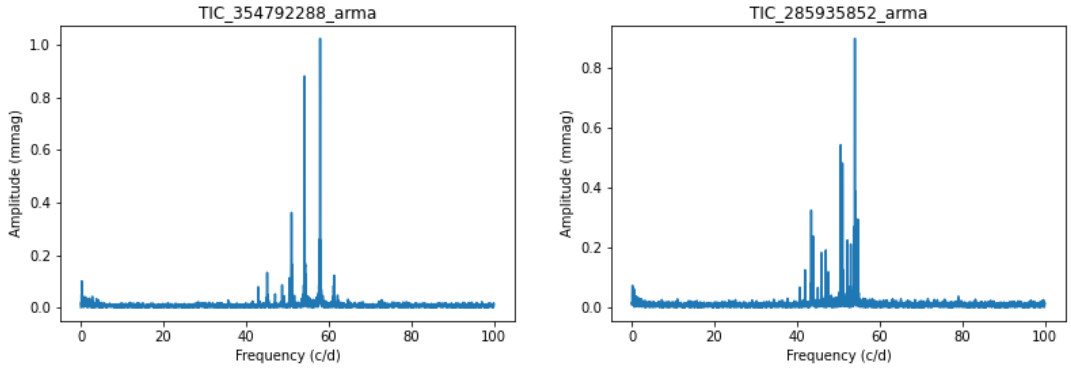

Figure 9. Periodograms for TIC 354792288 and TIC 285935852, showing a very grouped frequencies between 40 and 60 μHz

Table 4. Parameters of the selected targets. References: [1]Stassun et al. 2019, [2]Kounkel et al. 2019, [3]García Hernández et al. 2017, [4]Barceló Forteza et al., [5]Bowman & Kurtz 2018, [6]Barceló Forteza et al. 2020, [7]Hasanzadeh et al. 2021

TIC	$M(M_\odot)^1$	$R(R_\odot)^1$	$\bar{\rho}(\bar{\rho}_\odot)$	$logg^1$	$T_{\rm eff}(K)^1$	$log(L/L_\odot)^1$	$vsini(kms^{-1})^2$	$\Delta\nu_{\rm low}(cd^{-1})$	$\bar{\rho}_{\Delta\nu_{\rm low}}(\bar{\rho}_\odot)^3$	$T_{\nu_{max,0}}(K)^4$	$T_{\nu_{max,0}}(K)^5$	$T_{\nu_{max,w}}(K)^6$	$T_{\nu_{max,2D}}(K)^7$
410732825	[1.983:2.651]	[1.592:1.686]	[0.41:0.66]	[4.30:4.45]	[8851:9453]	[1.18:1.28]	[71:107]	[62:64]	[0.31:0.33]	-	-	-	-
354792288	[1.666:2.370]	[1.518:1.624]	[0.39:0.68]	[4.27:4.44]	[7849:8605]	[0.93:1.08]	[107:119]	[82:84]	[0.54:0.57]	[8202:9226]	[7883:8389]	[8351:8931]	[8255:8536]
285935852	[1.465:2.063]	[1.545:1.645]	[0.33:0.56]	[4.20:4.36]	[7363:7815]	[0.84:0.92]	[68:73]	[81:83]	[0.53:0.56]	[8099:9109]	[7808:8282]	[8202:8772]	[8183:8455]
252829836	[1.313:1.863]	[1.617:1.747]	[0.25:0.44]	[4.10:4.27]	[6994:7272]	[0.80:0.84]	[37:39]	[70:72]	[0.39:0.42]	-	-	-	-

Table 5. Constrained parameters of the models corresponding to our selected targets

TIC	$M(M_\odot)$	$R(R_\odot)$	$\bar{\rho}(\bar{\rho}_\odot)$	log g	$T_{\rm eff}$(K)	$log(L/L_\odot)$	Z_0	$v(kms^{-1})$	$\Delta\nu_{\rm low}(cd^{-1})$	Age (Myr)
410732825	[2.3:2.6]	[1.95:2.09]	[0.28:0.31]	[4.20:4.24]	[9731:10759]	[1.49:1.70]	[0.016:0.020]	[96:99]	[62:64]	[104:200]
354792288	[1.65:1.75]	[1.48:1.50]	[0.50:0.52]	[4.31:4.33]	[8192:8245]	[0.95:0.96]	[0.016:0.020]	[70:114]	[82:84]	[21:130]
285935852	[1.65:1.75]	[1.48:1.52]	[0.48:0.52]	[4.31:4.33]	[8202:8241]	[0.95:0.97]	[0.016:0.020]	[69:70]	[81:83]	[53:169]
252829836	[1.9:2.6]	[1.68:1.94]	[0.36:0.40]	[4.24:4.30]	[8541:11248]	[1.13:1.71]	[0.016:0.020]	[69:126]	[70:72]	[20:200]

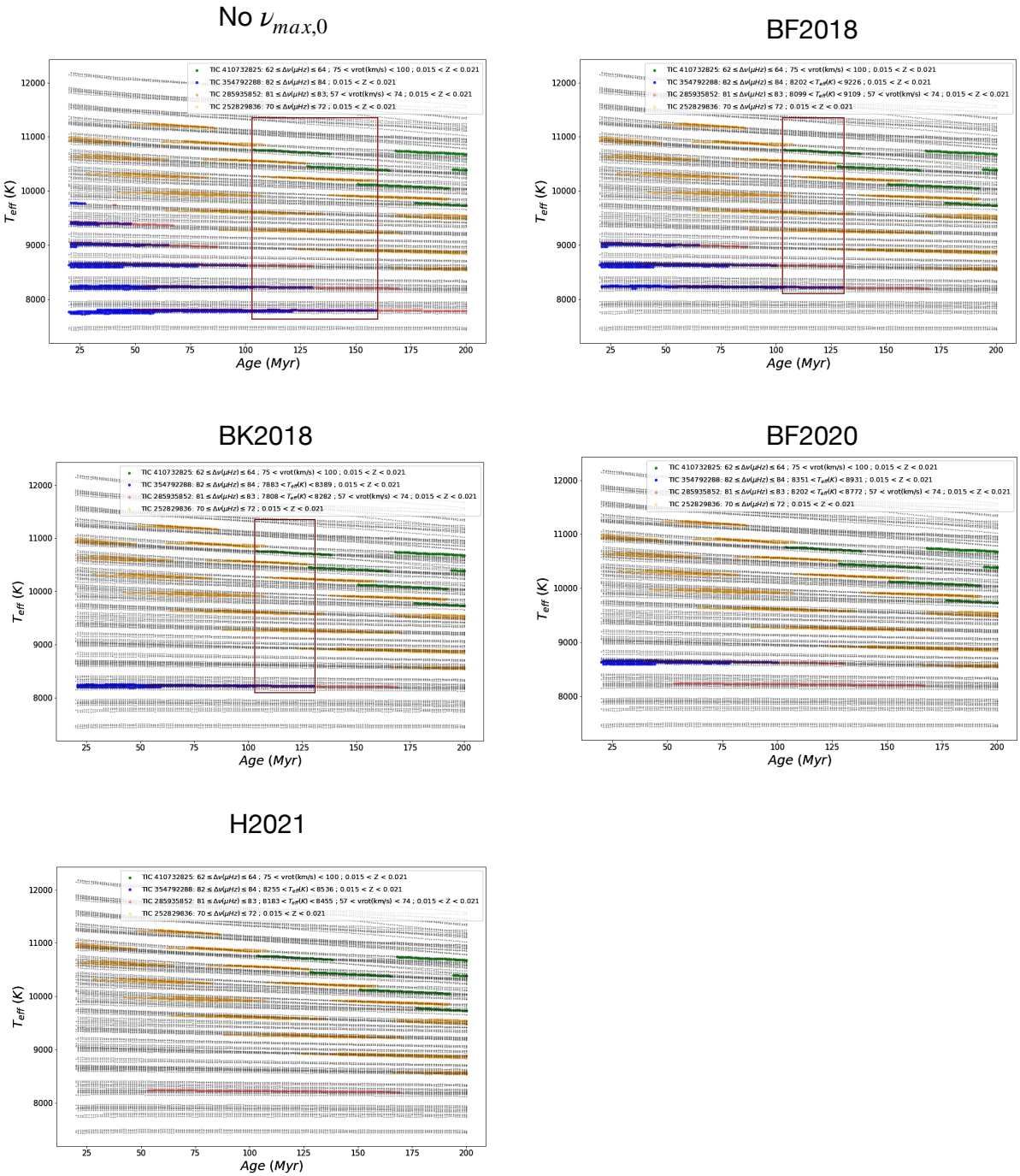

Figure 10. Constrained models for dating ages of the four stars, without using the relation between the frequency of maximum amplitude and effective temperature (No $\nu_{\max}$), and using the different relations of BF2018, BF2020, BK2018 and H2021

Balona L. A., 2014, MNRAS, 439, 3453

Balona L. A., Dziembowski W. A., 2011, MNRAS, 417, 591

Barceló Forteza S., Roca Cortés T., García Hernández A., García R. A., 2017, A&A, 601, A57

Barceló Forteza S., Roca Cortés T., García R. A., 2018, A&A, 614, A46

Barceló Forteza S., Moya A., Barrado D., Solano E., Martín-Ruiz S., Suárez J. C., García Hernández A., 2020, A&A, 638, A59

Bedding T. R., et al., 2020, Nature, 581, 147

Bowman D. M., Kurtz D. W., 2018, MNRAS, 476, 3169

Breger M., et al., 1993, A&A, 271, 482

Choi J., Dotter A., Conroy C., Cantiello M., Paxton B., Johnson B. D., 2016, ApJ, 823, 102

Dotter A., 2016, ApJS, 222, 8

Evano B., Lignières F., Georgeot B., 2019, Astronomy & Astrophysics, 631, A140

Gaia Collaboration et al., 2017, VizieR Online Data Catalog, pp J/A+A/601/A19

Gaia Collaboration et al., 2018, A&A, 616, A10

García Hernández A., et al., 2009, A&A, 506, 79

García Hernández A., Martín-Ruiz S., Monteiro M. J. P. F. G., Suárez J. C., Reese D. R., Pascual-Granado J., Garrido R., 2015, ApJ, 811, L29

García Hernández A., et al., 2017, MNRAS, 471, L140

Girardi L., Bressan A., Bertelli G., Chiosi C., 2000, A&AS, 141, 371
Grigahcène A., et al., 2010, ApJ, 713, L192
Hasanzadeh A., Safari H., Ghasemi H., 2021, MNRAS, 505, 1476
Heger A., Woosley S. E., Langer N., 2000, New Astron. Rev., 44, 297
Hey D., Ball W., 2020, Echelle: Dynamic echelle diagrams for asteroseismology, doi:10.5281/zenodo.3629933
Koch D. G., et al., 2010, ApJ, 713, L79
Kounkel M., et al., 2019, The Astronomical Journal, 157, 196
Lodieu N., Pérez-Garrido A., Smart R. L., Silvotti R., 2019, A&A, 628, A66
Makarov V. V., 2006, AJ, 131, 2967
Montgomery M. H., Odonoghue D., 1999, Delta Scuti Star Newsletter, 13, 28
Murphy S. J., Hey D., Van Reeth T., Bedding T. R., 2019, Monthly Notices of the Royal Astronomical Society, 485, 2380
Murphy S. J., Bedding T. R., White T. R., Li Y., Hey D., Reese D., Joyce M., 2021, arXiv e-prints, p. arXiv:2111.04203
Netopil M., Paunzen E., 2013, A&A, 557, A10
Paparó M., Benkő J. M., Hareter M., Guzik J. A., 2016, ApJ, 822, 100
Pascual-Granado J., Garrido R., Suárez J. C., 2015, A&A, 575, A78
Paxton B., 2019, Modules for Experiments in Stellar Astrophysics (MESA), doi:10.5281/zenodo.3473377
Paxton B., Bildsten L., Dotter A., Herwig F., Lesaffre P., Timmes F., 2011, ApJS, 192, 3
Paxton B., et al., 2013, ApJS, 208, 4
Paxton B., et al., 2015, ApJS, 220, 15
Pietrinferni A., Cassisi S., Salaris M., Castelli F., 2004, ApJ, 612, 168
Press W. H., Rybicki G. B., 1989, ApJ, 338, 277
Prosser C. F., 1992, AJ, 103, 488
Ramón-Ballesta A., García Hernández A., Suárez J. C., Rodón J. R., Pascual-Granado J., Garrido R., 2021, MNRAS, 505, 6217
Reegen P., 2007, Astronomy & Astrophysics, 467, 1353
Reese D. R., Lignières F., Ballot J., Dupret M.-A., Barban C., van 't Veer-Menneret C., MacGregor K. B., 2017, Astronomy & Astrophysics, 601, A130
Ricker G. R., et al., 2014, in Proc. SPIE. p. 914320 (arXiv:1406.0151), doi:10.1117/12.2063489
Scargle J. D., 1982, ApJ, 263, 835
Silaj J., Landstreet J. D., 2014, A&A, 566, A132
Stassun K. G., et al., 2019, The Astronomical Journal, 158, 138
Suárez J. C., Goupil M. J., 2008, Ap&SS, 316, 155
Suárez J. C., Goupil M. J., Morel P., 2006, Astronomy & Astrophysics, 449, 673
Suárez J. C., García Hernández A., Moya A., Rodrigo C., Solano E., Garrido R., Rodón J. R., 2014, A&A, 563, A7
Uytterhoeven K., et al., 2011, A&A, 534, A125
VanderPlas J. T., 2018, ApJS, 236, 16

A DIAGRAMS OF REGULARITIES OF THE OTHER THREE STARS

We include here the AC, FT, FDH and ED of TIC 410732825 (A.1), TIC 285935852 (A.2) and TIC 252829836 (A.3), which together with TIC 354792288 ((Figure 7), complete the four stars analyzed for which regularities have been found in their corresponding frequency spectra.

B COMPARATIVE ANALYSIS OF EFFICIENCY BETWEEN MM AND SS

Figure A.4 represents the executing time of both codes using the light curves of 11 δ Sct stars stars from our sample. MM is a factor two faster than SS in the cases where the number of extracted peaks is above 200 approximately.

This paper has been typeset from a TEX/LATEX file prepared by the author.

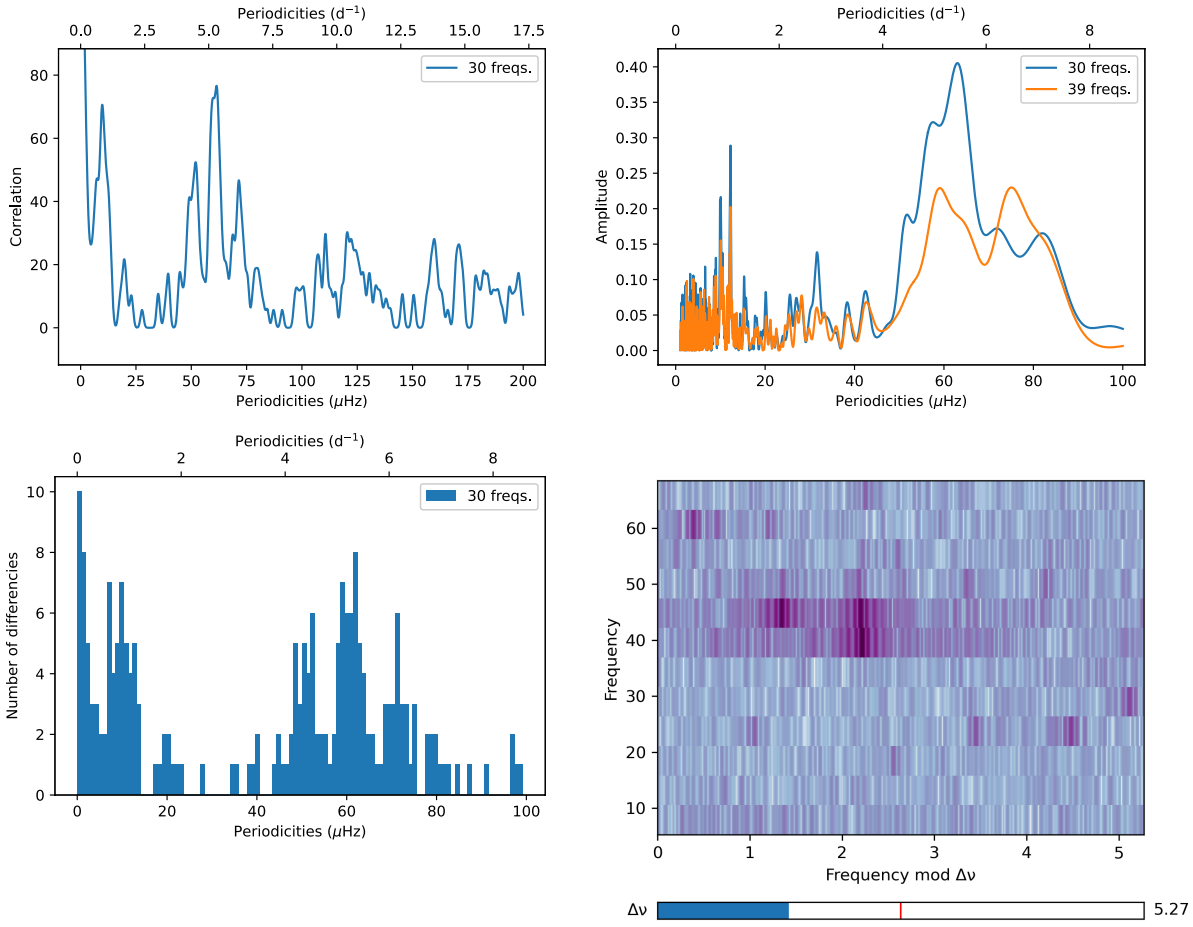

Figure A.1. Measured regularities for TIC 410732825

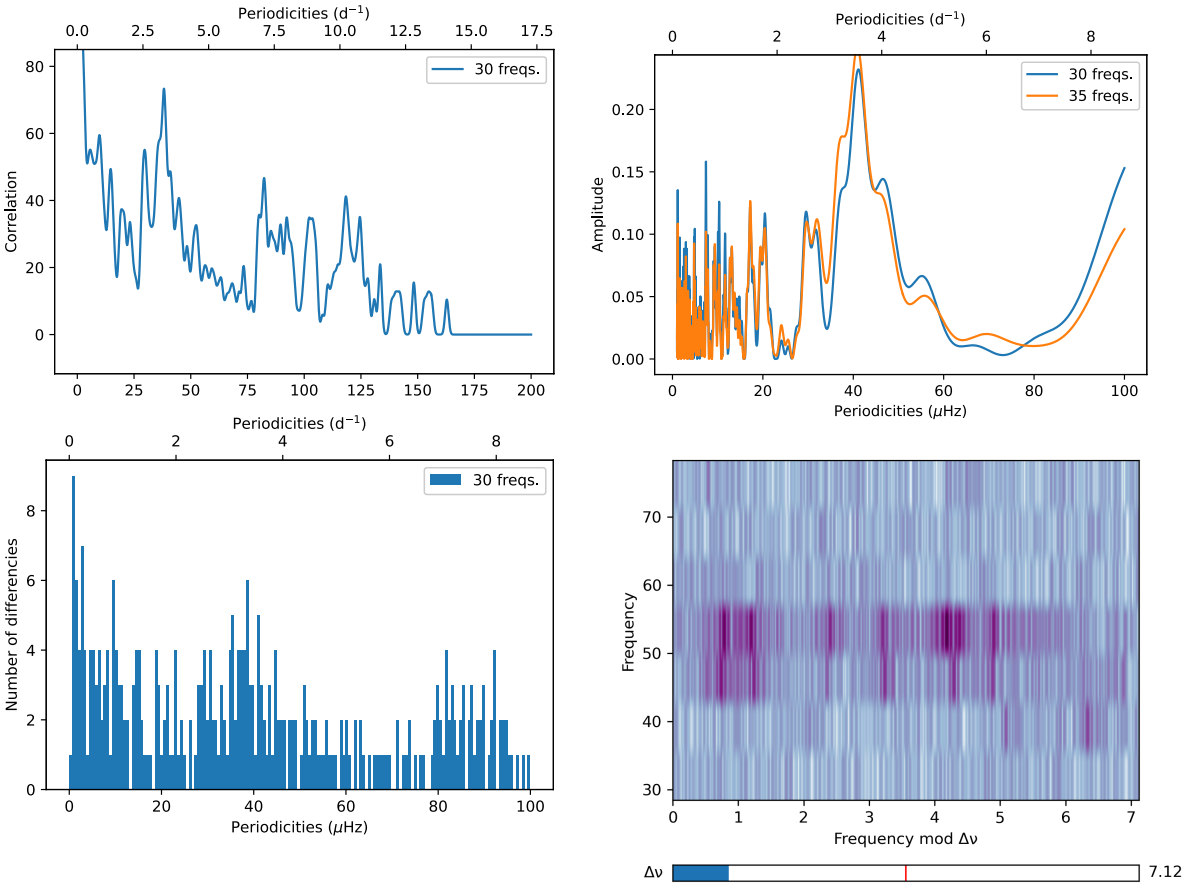

Figure A.2. Measured regularities for TIC 285935852

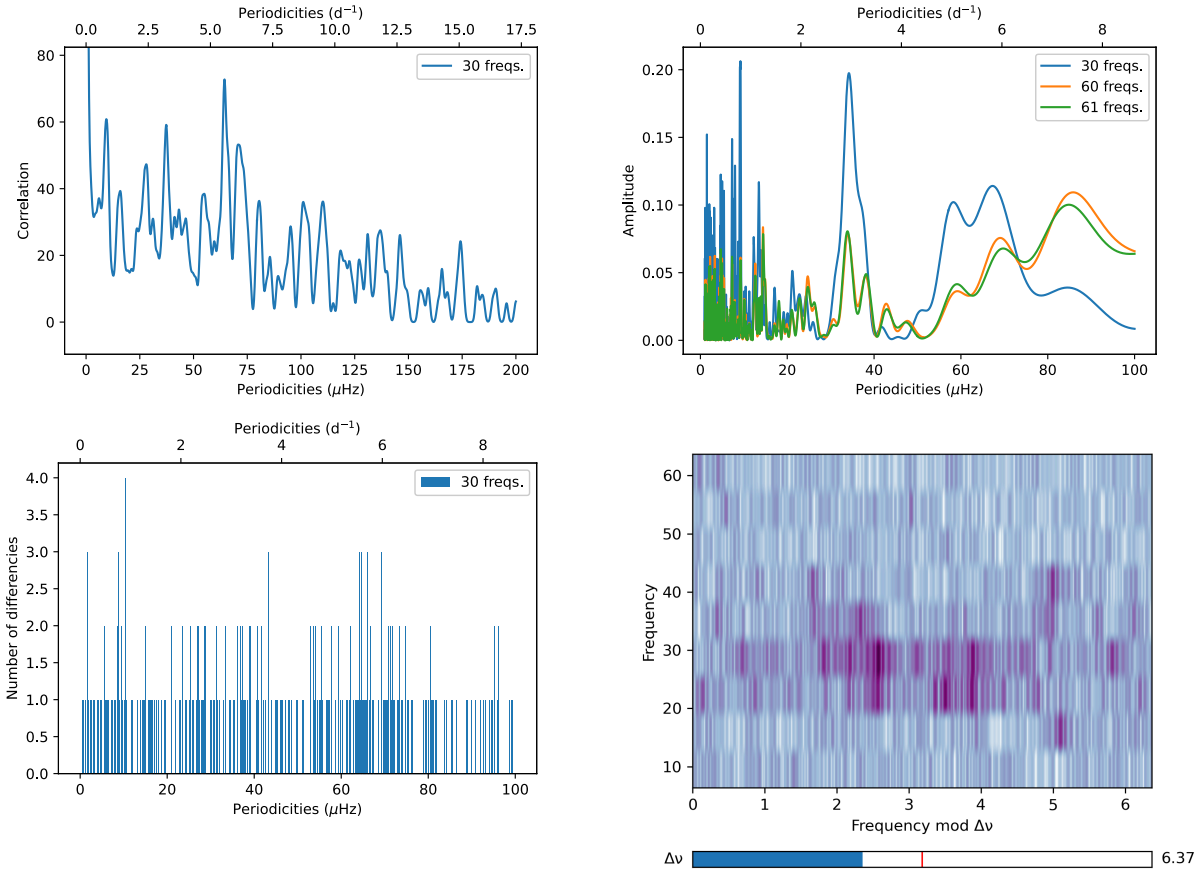

Figure A.3. Measured regularities for TIC 252829836

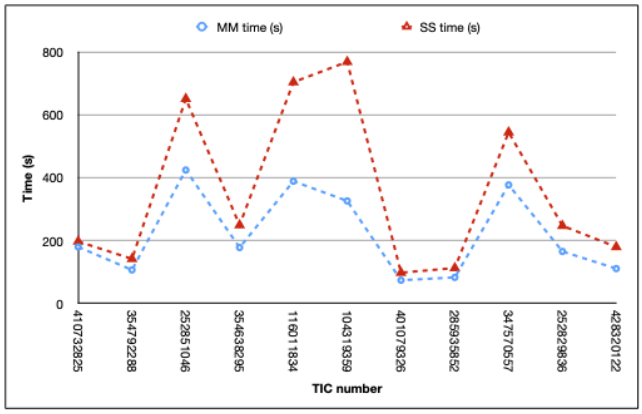

Figure A.4. Comparative analysis of efficiency between MM and SS, in terms of computing time, done with the sample of 11 δ Sct stars stars